Study of the interlayer adhesion and warping during material extrusion-based additive manufacturing of a carbon nanotube/biobased thermoplastic polyurethane nanocomposite

María Virginia Candal,[a,b*] Itxaso Calafel [b], Mercedes Fernández [b], Nora Aranburu [b], Roberto Hernández Aguirresarobe [b], Gonzalo Gerrica-Echevarria [b], Antxon Santamaría [b*] and Alejandro J. Müller [b,c*]

[a] Universidad Simón Bolívar, Departamento de Mecánica, Grupo de Polímeros, Apartado 89000, Caracas 1080-A, Venezuela

[b] POLYMAT and Faculty of Chemistry, University of the Basque Country UPV/EHU, Paseo Manuel de Lardizábal, 3, 20018 Donostia-San Sebastián, Spain.

[c] IKERBASQUE, Basque Foundation for Science, Bilbao, Spain

*Corresponding authors: mariavirginia.candalp@ehu.es, antxon.santamaria@ehu.es, alejandrojesus.muller@ehu.es

ABSTRACT

A thermoplastic bio-polyurethane from renewable sources (TPU) and the nanocomposite elaborated by mixing it with carbon nanotubes (CNT) are investigated as potentially adequate for Material Extrusion-based Additive Manufacturing (EAM). Thermal and rheological features are studied from the perspective of their liaisons with printing adequacy and conditions. As predicted by rheology, both samples show good performance in filament elaboration and flow in the nozzle. Warpage is observed for TPU, but not for the nanocomposite, which is explained considering differences in the crystallization process. According to our data, interlayer adhesion strength is independent of printing velocity (in the range employed), implying that there is no significant chain orientation that can induce changes in the TPU entanglements. The nanocomposite shows a lower welding strength, even though both have the same chain entanglements density. This is explained by considering that the higher viscosity of TPU/CNT, as compared to TPU, reduces the melt diffusion coefficient.

Key-words: thermoplastic polyurethane; carbon nanotubes; material extrusion-based additive manufacturing; entanglements; biobased TPU.

1. Introduction

Additive Manufacturing (AM) is the name given to emerging technologies that fabricate three-dimensional objects from a digital design by layer by layer material addition, as opposed to traditional subtractive techniques. For many years, AM was used only for rapid prototyping (RP) to obtain visualization models. Currently, AM is being used to fabricate end-use products in aerospace, automotive, construction, medical and dental implants, clothes and food, among others (1-2).

Extrusion-based additive manufacturing (EAM) is one of the seven 3D printing processes categories included in the ISO 17296-2 international standard. Filament fabrication (FFF) or fused deposition modeling (FDM) are two other names given to EAM in the field of plastics processing. EAM employs a continuous filament of a thermoplastic polymeric material that is fed from a large coil. A computer-aided design (CAD) software capable of creating "*.stl* files" that "slice" the part into thin layers is employed. This information drives the movement of a printer head and hot nozzle as they melt and add successive layers of material, forming a physical object on the heater bed (platform).

The reliability and simplicity of EAM technology have contributed to its wide spread use in industry and academia. Many researchers are working to improve the process, optimizing the process conditions, reducing the printing time, developing new materials, and applying the process in a wide range of engineering applications (3-5). Good adhesion between the deposited layers is very important for EAM parts. For this, the manufacture and process conditions used to obtain good quality and mechanical properties parts should be studied. The viscoelastic behavior when the polymer is melted and deposited to the bed (platform) is critical to perform good interlayer welding.

Some researchers have studied the effect of processing parameters and their optimization (6-10) on the mechanical properties of the printed parts (11-12). These studies are mostly focused on determining the optimum process conditions of EAM, to obtain adequate build time, mechanical resistance and surface integrity of the manufacturing parts. The mechanical resistance of parts made by EAM is usually lower than those manufactured by injection molding, because of their anisotropy and poorer adhesive strength between layers or filaments (13-16). Recently, Gao *et al.* (17) made an interesting review with the advances on bond interface in EAM pieces in aspects of its mechanisms, characterization and enhancement methods.

Amorphous thermoplastic polymers are the materials most commonly recommended for EAM. Their low thermal expansion coefficient and extrusion temperature reduce internal stresses presented during cooling (such as warping for example). But semi-crystalline polymers, such as polylactic acid (PLA), thermoplastic polyurethanes (TPU) and polyamides (PA) are currently employed for EAM. Specifically, TPUs are a class of polymers that provides a wide range of mechanical properties combined with physical and chemical properties (18). Although a number of papers refer to the processing of these polymers by EAM (19-21), indeed very few works have reported on the capacities and eventual advantages of this fabrication technique for TPUs filled with carbon nanotubes (CNTs), i.e., TPU/CNT nanocomposites. Christ *et al.* (22) demonstrated that TPU/MWCNT (multi-wall carbon nanotubes) nanocomposite is a material with excellent piezoresistive properties for EAM with potential electronic and medical applications. Li *et al*. (23), Kim *et al.* (24) and Gan *et al*. (25) prepared sensors with high piezoresistivity by using TPU/CNT fibers manufactured by EAM.

Notwithstanding the progress on the understanding of EAM of TPU and its nanocomposites, reflected in the aforementioned papers, the effect of carbon nanotubes on the following issues of TPU/CNT has not been studied, so far: a) Viscosity in the shear rate range involved in the nozzle; b) Interlayer welding, linked to polymer chains inter-diffusion between layers and, c) Dimensional stability of the final parts, linked to the phenomenon of warpage.

In this paper, we investigate the liaison between the basic physical properties of a biobased TPU/CNT nanocomposite and its performance in EAM, paying attention in particular to the current insufficiencies remarked in the previous paragraph. With this purpose, rheological measurements in linear and non-linear regime, as well as calorimetric and dilatometric experiments are performed to study the entanglements density and crystallization process. Taking advantage of the obtained results, the best conditions for EAM are established to elaborate dimensionally stable samples with remarkable interlayer adhesion. These results are interpreted considering the role played by polymer chains entanglements and the effect of CNTs on crystallinity and volume-temperature diagrams.

2. Materials and Methods

2.1 Materials

We employ a thermoplastic linear, aromatic bio-polyurethane (TPU) Pearlbond™ ECO 590 (MFI = 30–60 g/10 min, 170/2.16, ISO 1133) from Lubrizol (USA). It is based on a polyol from renewable sources. According to the results obtained by NMR (^{1}H and ^{13}C), it is composed of 4% methylene diphenyl 4,4'-diisocyanate (MDI) and 96% of poly(butylen sebacate) (PBSE).

A TPU based nanocomposite with 4 wt% CNT (TPU/CNT) was elaborated. Multi-wall carbon nanotubes (MWCNT Cheaptubes, China) of 20-30 nm outer diameter and 5-10 nm inside diameter, 10-30 microns in length and purity larger than 95% (information obtained of the data-sheet provided by the manufacturers) were used. A dehumidifier was used to dry the CNTs for 24h at 80°C before extrusion. TPU was also dried at 50ºC for 2 h in an air circulating oven. TPU and CNT were pre-mixed in the solid-state before feeding them to the extruder. Melt mixing of TPU with CNT was performed with a Collin ZK25 co-rotating twin-screw extruder-kneader, equipped with a 25 mm diameter screw and L/D ratio of 30. The extruder is equipped with 6 heating zones, and the programmed temperature profile was 120-120-125-125-130-130ºC. The screw rotation rate was 400 rpm. Extruded samples were quenched in a water bath and pelletized on-line, with a Collin CSG-171/1 pelletizer. The TPU/CNT pellets were dried in an air-circulating oven at 50°C for 24 h to remove moisture before further processing.

2.2 Elaboration of filaments

TPU and TPU/CNT filaments with 1.75 mm diameters for EAM were obtained with a Collin ZK25 co-rotating twin-screw extruder-kneader (screw diameter of 25 mm and L/D ratio of 30), and equipped with a circular die of 2.5 mm of diameter. The programmed temperature profile was 120-120-125-125-130-130ºC, and the screw rotation rate was in this case 50 rpm. The filaments obtained from the extruder were quenched in a water bath and winded. The winding speed was optimized to obtain filaments with a constant diameter of 1.75 mm, suitable for EAM.

2.3 EAM of samples

As printed equipment, a TUMAKER Voladora V1 from Tumaker (Spain) EAM Machine was employed. The printer was controlled with the software Simplify3D by Creative Tools AB. The digital model of the parts was designed and converted to STL file format for EAM. The maximum printing size obtained, with a nozzle diameter of 0.4 mm, was 22 x 22 x 30 cm (length, width, and height, respectively). The filaments thus obtained had an average diameter of 1.75 mm.

2.4 Printing parameters

The EAM printing parameters are listed in Table 1. We employ the Taguchi experimental design method. The selected response variable to optimize was the trouser test tearing energy. The proposed design included three process variables with three-factor levels (low, medium, and high). Such variables are nozzle temperature (ºC), printing velocity (mm/s), and bed temperature (ªC). The levels of each printing parameter were specified based on the recommended processing temperatures values for the materials used. These variables were modified to obtain adequate printing conditions for good bonding and adhesion between layers, that lead to optimized trouser test tearing energies. Parts were printed with edge-on layers orientation. The layer height, infill density, raster orientation, and infill pattern setting were held fixed at 0.3 mm, 100%, 0°, and rectilinear, respectively. The nozzle diameter was 0.4 mm. Five specimens for each condition were printed. The experimental data were processed following the recommendations of section 2.6 (see below).

Table 1. EAM process conditions studied in this work.

Condition	Nozzle temperature (°C)	Bed Temperature (°C)	Printing Velocity (mm/s)
L11	80	30	10
M11	100	30	10
M12	100	30	15
M13	100	30	20
H11	120	30	10

2.5 Welding tear strength (Trouser Tear) Geometry

The ASTM D1938-14 test method (26) is normally used to determine the critical tearing force by employing a Mode III ("trouser tear") fracture test. This method has been modified previously by Candal *et al.* (27), Davis *et al.* (28) and Seppala *et al.* (29) to study the interfacial bonding strength of parts manufactured using EAM. The Tinkercad open source software was used to draw the geometry of the EAM specimens. The generated files were first exported as STL files and then imported to the EAM software (Simplify3D). Figure 1 shows the trouser test specimen dimensions. A pre-crack of 60 mm was made by inserting a 0.01 mm wide section of aluminum paper in between layers 41 and 42 during printing.

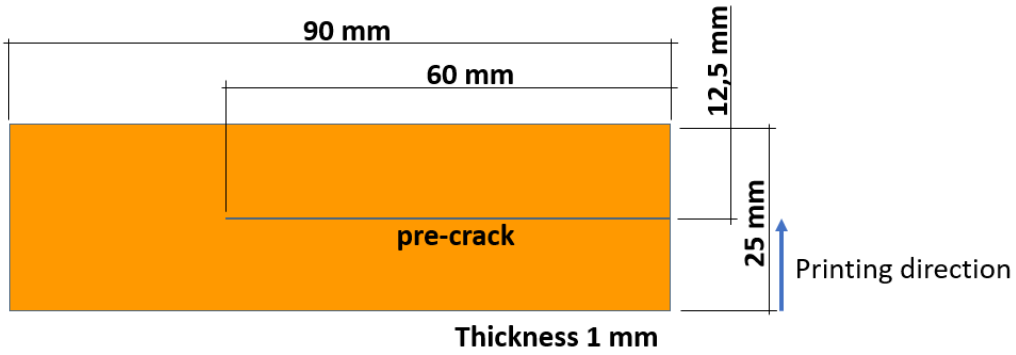

Figure 1: Dimensions of a trouser specimen.

2.6 Welding strength

Figure 2 shows a schematic illustrating a mode III fracture test or trouser tearing test. During this test, a force is applied to a polymer specimen that contains a pre-crack (generated during the molding of the sample, as indicated in Figure 1). The tearing energy of the EAM printed sample was obtained by modifying the ASTM D1938-14 test method (see references 27-29). The test was made with an INSTRON 5569 universal testing machine, employing 50 mm of initial distance, and a test speed of 254 mm/min. Pneumatic grips were used to hold the specimens during testing. The resulting tear force versus displacement curves for TPU and TPU/CNT are similar to those typically generated by low-extensible thin films and sheets (27). The average of the load over a 25.4 mm interval was used to calculate the tearing force.

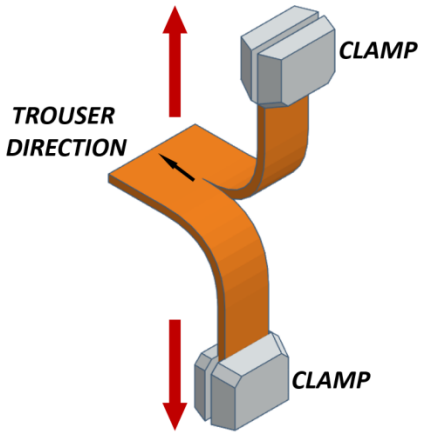

Figure 2: Trouser direction.

2.7 Thermal characterization of the materials

2.7.1. Differential scanning calorimetry (DSC)

The crystallization and melting temperatures of the polymers were measured with a Perkin-Elmer DSC 8000 equipped with an Intracooler 2. Ultra-pure nitrogen was used as purge gas. Samples with 7 mg of approximate weight were encapsulated in aluminum pans. Tin and indium standards were used as calibrants. Samples were first heated from 30°C to 100°C at a heating rate of 20°C/min; then, they were held at 100 ºC to erase thermal history, later they were cooled to 30 ºC at 20 ºC/min. After 3 minutes equilibration at 30 ºC, a second heating scan was recorded between 30 and 100 ºC. The degree of crystallinity, X_c, was calculated as:

$$X_c = \frac{\Delta H_m}{\Delta H_m^0 f} * 100 \qquad \text{(Eq. 1)}$$

where ΔH_m (J/g) is the experimentally obtained melting enthalpy of the sample, f is the fraction of the crystallizable phase (i.e., PBSE) and ΔH_m^0 is the equilibrium melting enthalpy. A value of ΔH_m^0=155±10 J/g reported by Papageorgiou *et al.* (30) for neat PBSE was employed.

2.7.2. Pressure–volume–Temperature (*PVT*) measurements

PVT behavior of TPU and TPU/ CNT was analyzed in a piston die type PVT100 equipment made by Haake (Germany). Experiments were performed from 120ºC to 0ºC. We performed isobaric cooling mode experiments (pressure range from 200-1600 bar) with a cooling rate of 5ºC/min. Employing the Tait model (32) to perform an extrapolation, we were able to obtain the results at a pressure of 1 bar. Several tests were performed to ensure that a volume difference lower than 0.05% between two measurements was achieved.

2.8 Rheology measurements

Capillary rheometry experiments were carried out in a Göttfert 2002 rheometer (with a capillary of D=1 mm and L=30 mm). The temperatures and shear rates employed are reported in the Results and Discussion section. Corrections for the non-Newtonian behaviour were performed, but pressure losses at the entrance were neglected, since a high length/diameter (L/D) die was employed. The viscosity as a function of shear rate, $\eta(\dot{\gamma})$, was obtained.

A stress-controlled TA Instruments ARG2 rheometer was employed for small amplitude oscillatory shear (SAOS) measurements with parallel-plates geometry (diameter 25 mm). Measurements were performed under nitrogen flow using TPU and TPU/CNT disks of 1 mm thickness. The elastic modulus, *G'*, and the viscous modulus, *G''* were measured in the linear viscoelastic regime (strain amplitude below 0.5%) in a frequency range of 0.01 to 100 Hz at varying temperatures from 70ºC to 150ºC.

2.9 Cross-section morphology

A Scanning Electron Microscope (SEM) (Hitachi S-2700) was employed to observe the weld between two filaments with 15 kV accelerating voltage. The specimens were fractured in liquid nitrogen, to avoid plastic deformation. Then the cross-sectional surface (the actual width of the weld) was gold (Au) coated with a Bio-Rad Microscience Division SC500 sputter Coater. The images of the printing filaments and the weld were captured with a digital camera. The thickness of the specimens ($2a_r$) were measured with an image analysis software *(Image J)*.

2.10 Weld tearing energy

The average tearing force (F_t) of the weld of two EAM layers was normalized with the nominal thickness of the specimen a_r to estimate the weld tearing energy (σ_t), following Davis *et al.* (28):

$$\sigma_t = \frac{F_t}{a_r} \qquad \text{(Eq. 2)}$$

3. Results and discussions

3.1. Rheological measurements

The viscosity results of TPU and TPU/CNT samples at 100 and 130ºC are presented in Figure 3. The data were fitted to a modified version of the Carreau-Yasuda equation (32):

$$\eta = \frac{\eta_o}{1+(\tau_o \dot{\gamma}^*_{21})^{\alpha}} \qquad \text{(Eq. 3)}$$

where η_o is the Newtonian viscosity, τ_o a relaxation time related to the onset of the disentanglement process and α a shear thinning index.

Notwithstanding that the viscosity values of the nanocomposites are considerably higher than those of neat TPUs, the difference is reduced as shear rate is increased. To relate the adequacy of these rheological results to the good performance of these materials in EAM, in Figure 3 we include the data of two commercial polymers widely used in EAM, such as PLA and ABS. Since the viscosities of both TPU and TPU/CNT samples lie in the range of the viscosities of the commercial specimens; we can assert that they are suitable to flow through the typical nozzle of an EAM device.

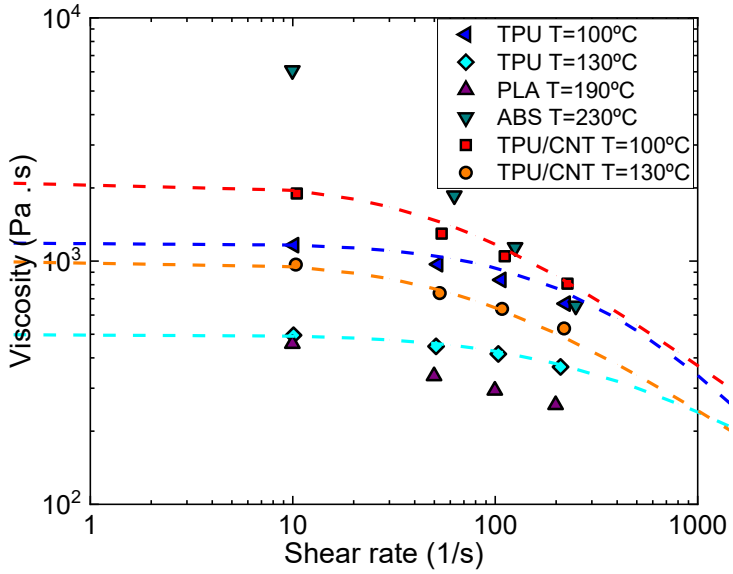

Figure 3. Flow curves (shear viscosity versus shear rate) of the investigated samples at T=100ºC and T=130ºC; the segmented lines correspond to fittings of equation 4. The results of PLA and ABS, commonly used for EAM, are also presented at their use temperatures for comparison purposes.

In recent years, some efforts have been made to correlate the viscoelastic properties of polymers to their interlayer welding performance once the melt is deposited in the bed (28-30). In particular, the role played by entanglements has been investigated, establishing a certain value for the entanglements density, above which interlayer adhesion is more efficient. Our analysis contemplates this point of view, as shown below.

The entanglements modulus, G_N^0, which is related to M_e, the molecular weight between entanglements, through the equation $M_e=\rho RT/G_N^0$, is calculated using the equation:

$$G_N^0 = \frac{2}{\pi}\int_{-\infty}^{+\infty} G''(\omega)\, d\ln\omega \qquad \text{(Eq. 4)}$$

The corresponding elastic and viscous moduli, G' and G'', as a function of frequency at T=70ºC, are presented in Figure 4. We choose this temperature as the intermediate between that of the nozzle and the bed. The results of the theory of the general linear viscoelastic fluids (33) are fulfilled for neat TPU, since the dependences $G'\sim\omega^2$ and $G''\sim\omega$ with $G''>G'$, are observed at low frequencies (below 0.1 Hz). This is a sign of the homogeneity of the neat

TPU that, as could be expected, is not obtained for the heterogeneous TPU/CNT nanocomposite.

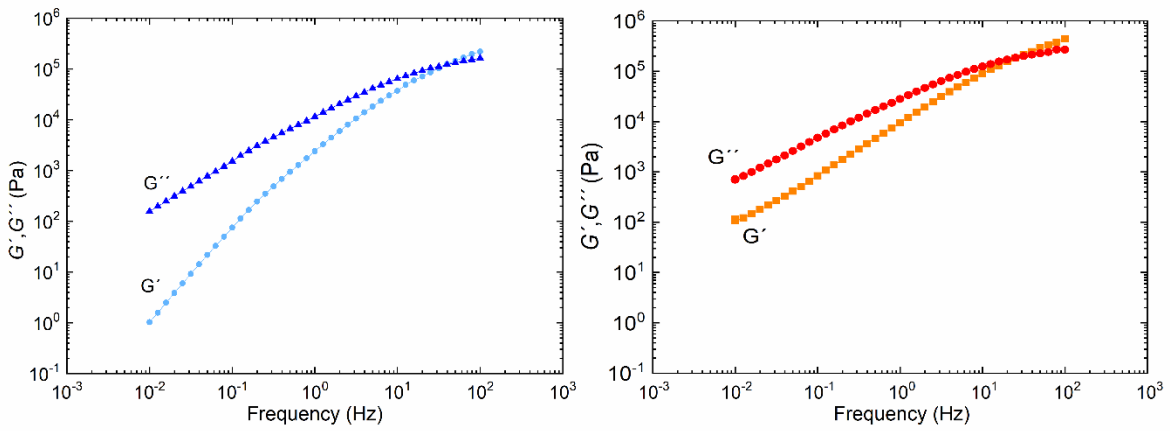

(a) (b)

Figure 4. Master curves of the elastic and viscous moduli at a reference temperature of 70ºC (a) TPU and (b) TPU/CNT.

We notice that for the nanocomposite also the viscous modulus prevails over the elastic modulus, $G''>G'$, except at frequencies close to 100 Hz at which the rubbery zone starts and $G'>G''$ for both samples. This result indicates that the rheological percolation, characterized by the suppression of the flow zone at low frequencies ($G'>G''$), has not been achieved in our TPU/CNT nanocomposite. Therefore, we assume that there is not a network formed by polymer chains-CNT interactions, so the only existing physical network in both samples is the entanglements network defined by G_N^0.

By means of equation 4 the entanglement modulus value for both samples is obtained: G_N^0= 1.45 MPa ± 0.07 MPa for TPU and G_N^0= 1.60 MPa ± 0.07 MPa for the TPU/CNT nanocomposite. Considering the relationship between the entanglements modulus and M_e, $M_e=\rho RT/G_N^0$, and the corresponding densities ρ= 0.985 g/cm^3 for TPU and ρ=1.038 g/cm^3 for TPU/CNT, obtained at T=70ºC by *PVT* tests (see section 3.2), the respective values are M_e=1950 g/mole for TPU and M_e=1875 g/mole for TPU/CNT. Therefore, the entanglements density, which is proportional to M_w/M_e, is alike for both samples. On the sole consideration of the similitude of the entanglement densities, similar values for the interlayer adhesion can be expected for TPU and TPU/CNT nanocomposite. This issue is discussed in Section 3.3 of the paper.

From another point of view, it should be noted that $G''>G'$ for both samples (Figure 4) which is a favorable condition for interlayer bonding, because inter-diffusion is more likely to occur under terminal or flow conditions. Although this is an acceptable general hypothesis, we note that it lies in contradiction with the proven good interlayer adhesion in ABS samples in EAM that show $G'>G''$ at low frequencies (28). As an alternative to this contradiction, we have recently proposed to use the Dalquist criterion (32), developed to analyze the immediate stickiness of adhesives, which states that the shear elastic modulus should be $G'< 3x10^5$ Pa at a frequency of 1 Hz to ensure good performance. The results shown in the Supporting Information, Figure 4, reveal that this requirement is satisfied by our samples at 70 ºC.

3.2 Differential Scanning Calorimetry (DSC)

DSC results at 20ºC/min are shown in Figure 5. The relevant calorimetric parameters are listed in Table 2. Figure 5 shows that both neat TPU and the TPU/CNT nanocomposite exhibit single crystallization and melting peaks.

As could be expected (34-35) a nucleating effect of the carbon nanotubes is observed as crystallization is accelerated, although the crystallinity degree of the TPU with and without nanotubes is very similar under the applied crystallization conditions**.** Interestingly enough, the shift of the crystallization temperature from 39 to 46ºC when CNTs are added to TPU has a crucial practical relevance, since it affects the dimensional stability of the specimens printed when the bed is at T=30ºC. In fact, noticeable warpage is observed for pure TPU, but not for the TPU/CNT composite.

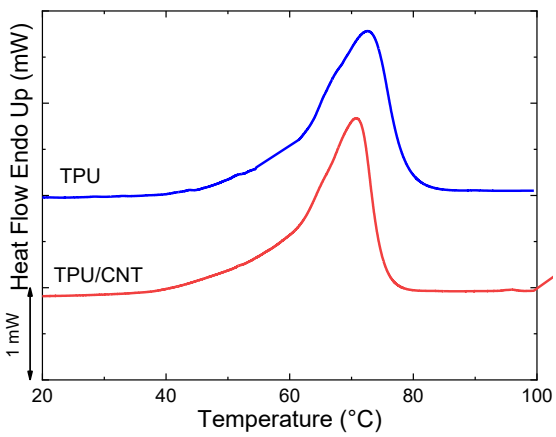

(a)

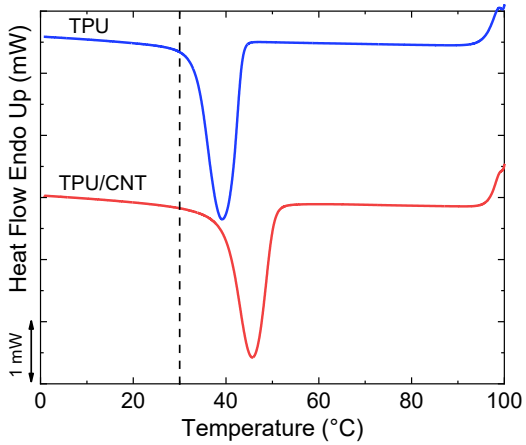

(b)

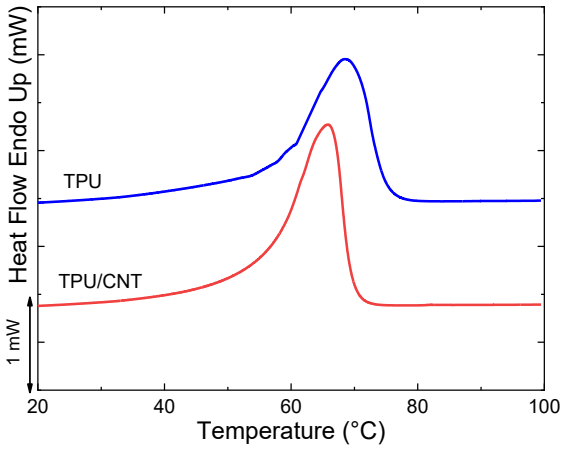

(c)

Figure 5. (a) DSC scans obtained during the first heating, (b) cooling and (c) second heating of filament samples of TPU and TPU/CNT. The vertical line drawn in b) corresponds to the printer bed temperature.

Table 2. Melting and crystallization temperatures (taken at the respective peaks), enthalpies and crystallinity degrees determined from DSC curves of TPU and TPU/CNT filaments.

	First heating			Cooling			Second heating		
Material	T_{m1} (°C)	ΔH_μ (J/g)	X_c (%)	T_c (°C)	ΔH_χ (J/g)	X_c (%)	T_{m2} (°C)	ΔH_μ (J/g)	X_c (%)
TPU	73	80.5	52	39	66.5	43	69	68.0	44
TPU/CNT	71	79.1	51	46	68.3	44	66	72.1	46

PVT results at a pressure of 1 bar, and a cooling rate of 5 ºC/min are shown in Figure 6. Analysis of the data in this figure shows that from 100ºC to 30ºC there is more volume reduction for TPU, ΔV=0.1105 cm^3/g, than for TPU/CNT, ΔV=0.0856 cm^3/g. Also, we found a higher contraction coefficient for TPU, $(dV/dT)1/V$= 7.6 10^{-4} ºC^{-1}, with respect to 5.5 10^{-4} ºC^{-1} for TPU/CNT in the range 20-35ºC. The relatively higher dimensional stability found for TPU/CNT nanocomposite samples is associated with the presence of carbon nanotubes that also contribute to avoiding the warpage effect, which is indeed observed in the case of TPU during EAM.

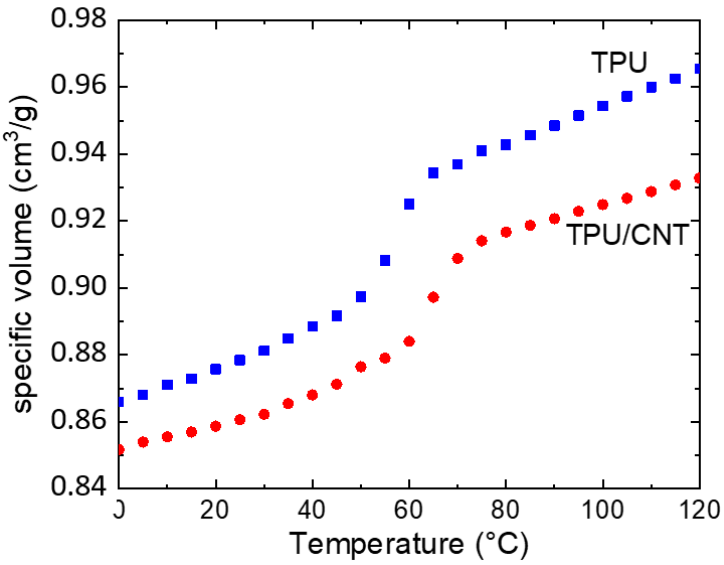

Figure 6. PVT cooling scans, at a pressure of 1 bar and a rate of 5 ºC/min, of non-processed (a) TPU and (b) TPU/CNT samples.

3.3 Strength of welding: Trouser tests

The trouser tear tests (Mode III) were implemented to study the fracture strength of the weld line of the printed specimens. The force vs. crosshead displacement curve allows the determination of the average tearing force at the EAM conditions. Examples of the representative force versus displacement curves of both materials for the same printing conditions are shown in Figure 7.

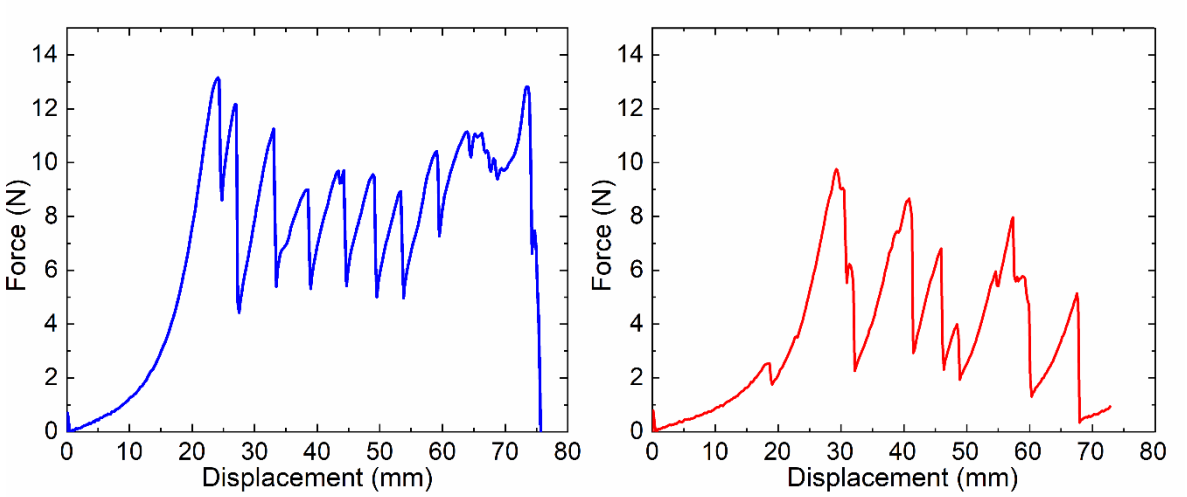

(a) (b)

Figure 7. Representative cases of force versus displacement curves (tear test) of (a) TPU and (b) TPU/CNT samples, 3D printed at nozzle and bed temperatures of 100ºC and 30ºC and with a printing velocity of 15 mm/s.

In our case, we followed the analysis of Davis *et al.* (27), and we determined the tearing energy dividing the average force value during steady state-crack propagation by the nominal thickness of the specimens ($2a_r$) / 2 after EAM, as previously indicated in equation 2. The nominal thickness of welded filaments, a_r, was determined by SEM micrographs, like those shown in Figure 8. The tearing energy results of the specimens printed under different EAM conditions are presented in Tables 3 and 4, the first reports the effect of printing velocity and the second the effect of nozzle temperature.

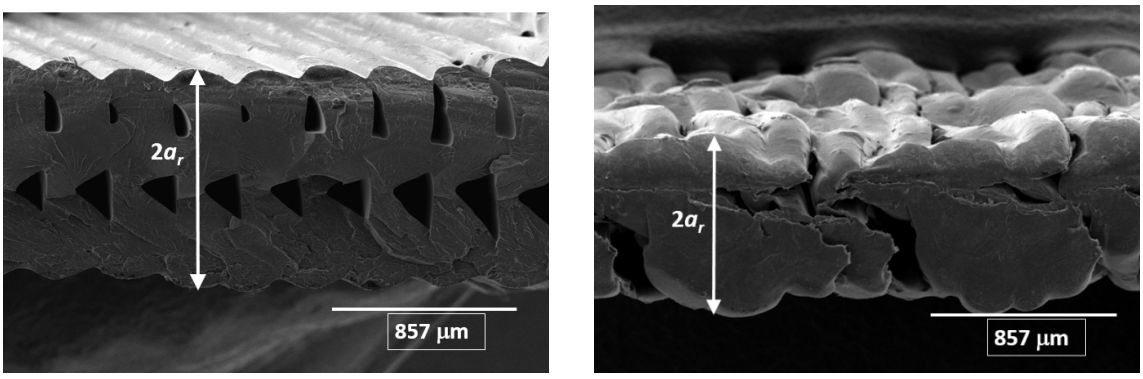

(a) (b)

Figure 8. SEM microphotographs of the fracture surface of 3D printed specimens of (a) TPU and (b) TPU/CNT. 3D printed conditions: melt temperature of 100ºC and bed temperature of 30ºC and 10 mm/min printing velocity.

Table 3. Tearing energy versus printing velocity for TPU and TPU/CNT with a bed temperature of 30°C and a nozzle temperature of 100°C.

		TPU	TPU/CNT
Condition	Printing velocity (mm/s)	Trouser energy (N/mm)	Trouser energy (N/mm)
M11	10.0	16.0 ±1.0	10.4±0.5
M12	15.0	15.3±0.9	10.7±0.9
M13	20.0	15.3±0.3	11.4±1.0

To analyze the results, we need to consider the recent research of McIlroy *et al.* (36-37) on the effect of disentanglements on weld strength, promoted by chain alignment at the weld interface. In the model of McIlroy *et al.*, the role played by polymer chains inter-diffusion at the interface is relegated due to the dominant effect of the non-equilibrium configuration of the entanglements. Alignment is enhanced as printing velocity is increased, and the experimentally observed consequence of this is a reduction of the weld strength and tearing energy.

Table 4. Tearing energy versus nozzle temperature of TPU and TPU/CNT with a bed temperature of 30°C and a printing velocity of 10 mm/s.

		TPU	TPU/CNT
Condition	Nozzle temperature (°C)	Tearing energy (N/mm)	Tearing energy (N/mm)
L11	80	5.5±0.3	4.0±0.1
M11	100	16.0±1.0	10.4±0.5
H11	120	18.5±1.2	14.0±0.1

According to the results reported by McIllroy *et al.* (36-37) for polycarbonate and PLA, printing velocities higher than 20 mm/s are required to observe the weld strength decrease due to chain orientation effects. Thus, the lower printing velocity values (<20 mm/s) employed in our EAM processes to obtain the TPU and TPU/CNT specimens can explain the absence of any particular effect of printing velocity on the tearing energies of both samples seen in Tables 3-4. Other authors (38-39) obtained similar results upon variation of printing velocity. Consequently, it can be assumed that our welding strength results arise from inter-diffusion of the polymer chains across filament-filament interface, rather than from disentanglements due to alignment (40-41). The enhancing effect of temperature on welding and the lower tearing energy values found for TPU/CNT with respect to pure TPU, observed in Table 4, support this assumption.

Although a mathematical relation between the tearing energy and the polymer diffusion coefficient has not been yet established, it is assumed that the larger the polymer diffusion, the stronger the welding. Coupling polymer diffusion and rheological results was

a task developed years ago, for instance, by Qiu and Bousmina (42). In particular, the dependence of the diffusion coefficient on the Newtonian viscosity can be expressed as (35):

$$\Delta_\chi \cong M_\varepsilon \rho R\ T/\eta_o \quad \text{(Eq. 5)}$$

where M_e is the entanglement molecular weight, ρ the density, R the gas constant, and η_o the Newtonian viscosity.

A temperature increase leads to enhanced diffusion through the observed direct proportionality in the equation and also via viscosity reduction, so the significant enhancement of tearing energy observed as a function of temperature (Table 4) should be associated with the increase in the diffusion coefficient. Equation 5 also explains the higher tearing energies of TPU, as compared to TPU/CNT. As shown in Figure 3, lower viscosities are obtained in the former, which implies larger diffusion coefficient values and, consequently, larger tearing energies.

4. Conclusions

The comparative thermal and rheological analysis of a biobased TPU and its nanocomposite with 4% carbon nanotubes, TPU/CNT, reveals that both samples are adequate for EAM. Nevertheless, the following differences are noticed: I) The viscosity is higher for TPU/CNT (particularly at low shear rates), but lies in the range of viscosities of other thermoplastics used for EAM; II) At the processing temperatures and at low frequencies, the elastic modulus, G', is higher for the nanocomposite, but the entanglement modulus and M_e are similar for both samples; III) the 3D printed TPU sample shows a slight warpage in the bed, not observed in TPU/CNT sample; IV) The interlayer adhesion, as measured by the tearing experiment, is lower for TPU/CNT nanocomposite.

The absence of warpage in the TPU/CNT nanocomposite is due to its higher dimensional stability, which resulted from its higher solidification temperature caused by the nucleating effect of the CNTs. The lower interlayer welding strength is regarded to be due to the higher viscosity of TPU/CNT at low shear rates, which leads to a lower chain interdiffusion between layers.

Considering the advantages and flaws of the investigated nanocomposite, the paper overall constitutes a case of a thermal and rheological study to investigate the reliability of filled polymers to be processed by EAM.

Acknowledgment

We would like to thank the financial support provided by the BIODEST project. This project has received funding from the European Union's Horizon 2020 research and innovation programme under the Marie Skłodowska-Curie grant agreement No 778092. This work has also received funding from MINECO through project MAT2017-83014-C2-1-P and from the Basque Government through grant IT1309-19.

References

1. I. Gibson, D. Rosen, B. Stucker., Additive Manufacturing Technologies: 3D Printing, Rapid Prototyping, and Direct Digital Manufacturing, Springer, Cincinnati, 2015.

2. Ch. Kai, K. Fai, K., 3D Printing and Additive Manufacturing: Principles and Applications, World Scientific Publ., New York, 2016.

3. Q. Sun, G. Rizvi, C.T. Bellehumeu, P. Gu, P. Gu, Effect of processing conditions on the bonding quality of FDM polymer filaments. Rapid Prototyping Journal 14 (2) (2008) 72-80. DOI: 10.1108/13552540810862028.

4. J. W. Comb, W.R. Priedeman, P.W. Turley, Layered manufacturing control parameters and material selection criteria, Journal of Manufacturing Science and Engineering 68-2 (2002) 547-556. ISBN: 0791814351.

5. S. Allen, D. Dutta, Wall thickness control in layered manufacturing for surfaces with closed slices. Computational geometry, Theory and Applications 10(4) (1998) 223–238. https://doi.org/10.1016/S0925-7721(98)00009-1.

6. P. Alexander, D. Dutta, Layered manufacturing of surfaces with open contours using localized wall thickening, Computer Aided Design 32 (3) (2000) 175-189. https://doi.org/10.1016/S0010-4485(99)00079-2.

7. W.B. Han, M.A. Jafari, K. Seyed, Process speeding up via deposition planning in fused deposition-based layered manufacturing processes, Rapid Prototyping Journal 9 (4) (2007) 212-218. https://doi.org/10.1108/13552540310489596.

8. Yadav, D., Chhabra, D., Kumar Garg, R., Ahlawat, A., Phogat, A., (2019), Optimization of FDM 3D printing process parameters for multi-material using artificial neural network. Materials Today: Proceedings. doi:10.1016/j.matpr.2019.11.225.

9. G. Budzik, Geometric accuracy of aircraft engine blade models constructed by means of generative rapid prototyping methods FDM and SLA, Advances in Manufacturing Science and Technology 34(1) (2010) 33-43.

10. A. García-Domínguez, J. Claver, M.A. Sebastián, Methodology for the optimization of work pieces for additive manufacturing by 3D printing. Procedia Manufacturing 13 (2017) 910-915. https://doi.org/10.1016/j.promfg.2017.09.158.

11. J.F. Rodríguez, J. Thomas, J. Renaud, Mechanical behavior of acrylonitrile butadiene styrene (ABS) fused deposition materials. Experimental investigation, Rapid Prototyping Journa, 7(3) (2001) 148-158. DOI: 10.1108/13552540310489604.

12. R. Munprom, S. Limtasiri, Optimization of stereolithographic 3D printing parameters using Taguchi method for improvement in mechanical properties, Materials Today Proceedings 17(4) (2019) 1768-1773. https://doi.org/10.1016/j.matpr.2019.06.209.

13. R. Anitha, S. Arunachalam, P. Radhakrishnan, Critical parameter influencing the quality of prototype in fused deposition modeling, Journal of Materials Processing Technology 118 (1-3) (2001), 385–388. DOI: 10.1016/S0924-0136(01)00980-3.

14. C.J. Luis, Analysis of the surface roughness and dimensional accuracy capability of fused deposition modelling processes, International Journal of Production Research 40(12) (2001) 2865–2881. https://doi.org/10.1080/00207540210146099.

15. P.M. Pandey, N.V. Reddy, S.G. Dhande, Real time adaptive slicing for fused deposition modeling, International Journal of Machine Tools and Manufacture 43 (1) (2003) 61–71. https://doi.org/10.1016/S0890-6955(02)00164-5.

16. M. Lay, N. Najwa, Z. Abdul, A. Rusli, M. Khalil, R. Shuib, Comparison of physical and mechanical properties of PLA, ABS and nylon 6 fabricated using fused deposition modeling and injection molding, Composites Part B: Engineering 176(1) (2019) 107341. https://doi.org/10.1016/j.compositesb.2019.107341.

17. X. Gao, S. Qi, X. Kuang, Y. Su, J. Li, D. Wang, Fused Filament Fabrication of Polymer Materials: A Review of Interlayer Bond. Additive Manufacturing October (2020), 101658. doi:10.1016/j.addma.2020.101658.

18. H.J. Qi, M.C. Boyce, Stress–strain behavior of thermoplastic polyurethanes. Mechanics of Materials 37(8) (2005) 817-839. https://doi.org/10.1016/j.mechmat.2004.08.001.

19. S. Bates, I.R. Farrow, R. Trask, 3D printed polyurethane honeycombs for repeated tailored energy absorption, Materials & Design 112(15) (2016) 172-183. https://doi.org/10.1016/j.matdes.2016.08.062.

20. J. Xiao, Y. Gao, The manufacture of 3D printing of medical grade TPU, Progress in Additive Manufacturing 2(3) (2017) 117–123. DOI:10.1007/s40964-017-0023-1.

21. A. S. De León, A. Domínguez-Calvo, S. I. Molina, Materials with enhanced adhesive properties based on acrylonitrile-butadiene-styrene (ABS)/thermoplastic polyurethane (TPU) blends for fused filament fabrication (FFF), Materials & Design 182 (2019) 108044. DOI:10.1016/j.matdes.2019.108044.

22. Ch. Christ, N. Aliheidari, A. Amelia, P. Pötschke, 3D printed highly elastic strain sensors of multiwalled carbon nanotube/thermoplastic polyurethane nanocomposites. Materials & Design 131(5) (2017) 394-401. https://doi.org/10.1016/j.matdes.2017.06.011.

23. Z. Li, Z. Wang, X. Gan, D. Fu, G. Fei, H. Xia, Selective laser sintering 3D printing: a way to construct 3D electrically conductive segregated network in polymer matrix, Macromol. Mater. Eng. 302 (2017), 1700211. https://doi.org/10.1002/mame.201700211.

24. K. Kim, J. Park, J. Suh, M. Kim, Y. Jeong, I. Park. 3D printing of multiaxial force sensors using carbon nanotube (CNT)/thermoplastic polyurethane (TPU) filaments, Sensors and Actuators A: Physical 263(15) (2017) 493-500. https://doi.org/10.1016/j.sna.2017.07.020.

25. X. Gan, J. Wang, Z. Wang, Z. Zheng, M. Lavorgna, A. Ronca, G. Fei, H. Xia, Simultaneous realization of conductive segregation network microstructure and minimal surface porous macrostructure by SLS 3D printing, Materials & Design 178(15) (2019) 107874. https://doi.org/10.1016/j.matdes.2019.107874.

26. Standard ASTM D1938 – 19, Standard Test Method for Tear-Propagation Resistance (Trouser Tear) of Plastic Film and Thin Sheeting by a Single-Tear Method, EEUU.

27. M. V. Candal, I. Calafel, N. Aranburu, M. Fernández, G. Gerrica-Echevarria, A. Santamaría, A. J. Müller, 3D Printing semi-crystalline PBS and PBSA biodegradable polyesters: A thermo-rheological analysis focused on FFF, submitted to Additive Manufacturing (2020).

28. C. Davis, K. Hillgartner, S. Hoon Han, J. Seppala, Mechanical strength of welding zones produced by polymer extrusion additive manufacturing, Additive manufacturing 16 (2017) 162-166. https://doi.org/10.1016/j.addma.2017.06.006.

29. J. Seppala, S. Hoon Han, K. Hillgartner, C. Davis, K. Migl, Weld formation during material extrusion additive manufacturing, Soft Matter 13 (2017) 13 6761-6769. DOI: 10.1039/C7SM00950J.

30. G. Z. Papageorgiou, D. N Bikiaris, D. S. Achilias, S. Nanaki, N. Karagiannidis, Synthesis and comparative study of biodegradable poly (alkylene sebacate), Journal of Polymer Science Part B: Polymer Physics 48(6) (2010) 672-686. DOI: 10.1002/polb.21937.

31. P. Zoller, Y. A. Fakhreddine, Pressure-volume-temperature studies of semicrystalline polymers, Thermochimica Acta (1994) 238 (June) 397-415. https://doi.org/10.1016/S0040-6031(94)85221-9.

32. R. Byron Bird, Robert C. Armstrong, O. Hassager, Dynamics of Polymeric Liquids, Volume 1: Fluid Mechanics, 2nd Edition; John Wiley and Sons Inc., New York, 1987.

33. I. Calafel, R. H. Aguirresarobe, M. I. Peñas, A. Santamaria, M. Tierno, J. I. Conde, B. Pascual, Searching for Rheological Conditions for FFF 3D Printing with PVC Based Flexible Compounds, Materials 13(1) (2020) 178. https://doi.org/10.3390/ma13010178.

34. F. Avalos-Belmontes, L. F. Ramos-deValle, E. Ramírez-Vargas, S. Sánchez-Valdes, J. Méndez-Nonel, R. Zitzumbo-Guzmán, Nucleating Effect of Carbon Nanoparticles and Their Influence on the Thermal and Chemical Stability of Polypropylene, Journal of Nanomaterials October (2012) 1–8. DOI:10.1155/2012/406214.

35. S. Barrau, C. Vanmansart, M. Moreau, A. Addad, G. Stoclet, J.M. Lefebvre, R. Seguela, R., Crystallization Behavior of Carbon Nanotube−Polylactide Nanocomposites, Macromolecules 44(16) (2011) 6496–6502. DOI:10.1021/ma200842n.

36. C. McIlroy, P.D. Olmsted, Disentanglement effects on welding behaviour of polymer melts during the fused-filament-fabrication method for additive manufacturing, Polymer 123 (11) (2017) 376-391. https://doi.org/10.1016/j.polymer.2017.06.051.

37. A. Costanzo, R. Spotorno, M.V. Candal, M. Fernández, A. J. Müller, R. Graham, D. Cavallo, C. McIlroy, Residual alignment and its effect on weld strength in MatEx-printed polylactic acid, Additive Manufacturing 36 (2020), 101415.

38. M. A. Cunha, M. O. Robbins, Effect of Flow-Induced Molecular Alignment on Welding and Strength of Polymer Interfaces. Macromolecules 53 (19) (2020), 8417–8427. https://dx.doi.org/10.1021/acs.macromol.0c01508?ref=pdf.

39. T. J. Coogan, D. O. Kazmer, Prediction of interlayer strength in material extrusion additive manufacturing, Additive Manufacturing 35 (2020), 101368. https://doi.org/10.1016/j.addma.2020.101368.

40. X. Gao, S. Qi, D. Zhang, Y. Su, D. Wang, The role of poly (ethylene glycol) on crystallization, interlayer bond and mechanical performance of polylactide parts fabricated by fused filament fabrication, Additive Manufacturing, 35 (2020), 101414. DOI: 10.1016/j.addma.2020.101414.

41. T. C. Yang, C.H. Yeh, Morphology and Mechanical Properties of 3D Printed Wood Fiber/Polylactic Acid Composite Parts Using Fused Deposition Modeling (FDM): The Effects of Printing Speed. Polymers, 12(6) (2020), 1334. DOI: 10.3390/polym12061334.

42. H. Qiu, M. Bousmina, New technique allowing the quantification of diffusion at polymer/polymer interfaces using rheological analysis: Theorical and experimental results, Journal of Rheology 43 (3) (1999) 551-568. DOI: 10.1122/1.550904.